



Chinese Pharmaceutical Association
Institute of Materia Medica, Chinese Academy of Medical Sciences

Acta Pharmaceutica Sinica B

www.elsevier.com/locate/apsb
www.sciencedirect.com



ORIGINAL ARTICLE

(+)/(–)-Gerbeloid A, a pair of unprecedented coumarin-based polycyclic meroterpenoid enantiomers from *Gerbera piloselloides*: Structural elucidation, semi-synthesis, and lipid-lowering activity



Chenxu Zhao^{a,†}, Jingrong Li^{a,†}, Yue Hu^a, Lingyu Li^a, Meng Yu^a, Yunfeng Huang^b, Tao Zhang^{a,*}, Hai Shang^{a,*}, Zhongmei Zou^{a,*}

^aState Key Laboratory of Bioactive Substance and Function of Natural Medicines, Institute of Medicinal Plant Development, Chinese Academy of Medical Sciences & Peking Union Medical College, Beijing 100193, China

^bInstitute of Chinese Medicine Resources, Guangxi Institute of Chinese Medicine & Pharmaceutical Science, Nanning 530000, China

Received 14 October 2023; received in revised form 12 March 2024; accepted 20 March 2024

KEY WORDS

Gerbera piloselloides;
Natural products;
Coumarin meroterpenoid;
Structural elucidation;
Biomimetic synthesis;
Lipid-lowering activity;
3T3-L1 adipocytes;
High-fat diet zebrafish model

Abstract A pair of coumarin-based polycyclic meroterpenoid enantiomers (+)/(–)-gerbeloid A [(+)-**1a** and (–)-**1b**] were isolated from the medicinal plant *Gerbera piloselloides*, which have a unique caged oxatricyclo [4.2.2.0^{3,8}] decene scaffold. Their planar and three-dimensional structures were exhaustively characterized by comprehensive spectroscopic data and X-ray diffraction analysis. Guided by the hypothetical biosynthetic pathway, the biomimetic synthesis of racemic **1** was achieved using 4-hydroxy-5-methylcoumarin and citral as the starting material *via* oxa-6π electrocyclicization and intramolecular [2 + 2] photocycloaddition. Subsequently, the results of the biological activity assay demonstrated that both (+)-**1a** and (–)-**1b** exhibited potent lipid-lowering effects in 3T3-L1 adipocytes and the high-fat diet zebrafish model. Notably, the lipid-lowering activity of (+)-**1a** is better than that of (–)-**1b** at the same concentration, and molecular mechanism study has shown that (+)-**1a** and (–)-**1b** impairs adipocyte differentiation and stimulate lipolysis by regulating C/EBPα/PPARγ signaling and Perilipin signaling *in vitro* and *in vivo*. Our findings provide a promising drug model molecule for the treatment of obesity.

*Corresponding authors.

E-mail addresses: tzhang@implad.ac.cn (Tao Zhang), hshang@implad.ac.cn (Hai Shang), zmzou@implad.ac.cn (Zhongmei Zou).

†These authors made equal contributions to this work.

Peer review under the responsibility of Chinese Pharmaceutical Association and Institute of Materia Medica, Chinese Academy of Medical Sciences.

<https://doi.org/10.1016/j.apsb.2024.03.035>

2211-3835 © 2024 The Authors. Published by Elsevier B.V. on behalf of Chinese Pharmaceutical Association and Institute of Materia Medica, Chinese Academy of Medical Sciences. This is an open access article under the CC BY-NC-ND license (<http://creativecommons.org/licenses/by-nc-nd/4.0/>).

1. Introduction

Obesity, characterized by increased mass or functions of adipose tissue stores resulting from a chronic imbalance between energy intake and energy expenditure, has become a global epidemic and is a risk factor for various life-threatening diseases such as type 2 diabetes mellitus (T2DM), non-alcoholic fatty liver disease (NAFLD), non-alcoholic steatohepatitis (NASH), cardiovascular disease (CVD) and some kinds of cancer^{1–3}. For obese patients, lifestyle intervention, drug therapy, bariatric surgery, etc., are the main treatment methods⁴. However, due to poor patient compliance and strict indications for surgical treatment, the search for innovative weight-loss drugs is the ideal development direction for treatment⁵. Natural products have always played an important and irreplaceable role in the development of new drugs⁶. Therefore, mining novel types of molecules from natural products is a promising way to develop new drugs for obesity-related metabolic diseases.

5-Methylcoumarins belong to a member of the coumarin family, but unlike most coumarins, they are formed *via* pentaketide derived from the acetate-malonate pathway⁷. This rare type of coumarin typically contains a hemiterpene (C5), monoterpene (C10), or sesquiterpene (C15) residue at C-3 to form unique 5-methylcoumarin meroterpenoids⁸. Such natural products are not frequently found in natural sources but have been isolated from species of Mutisioideae (the subfamily of Compositae)⁹. Specifically, the 5-methylcoumarin meroterpenoids consisting of prenyl- and geranyl-substituted coumarin are predominant in species of the *Gerbera* and *Ainsliaea* DC genera (Mutisieae, the tribe of Mutisioideae)^{10–12}. Intuitively, 5-methylcoumarin meroterpenoids with a monoterpene framework may be related to traditional efficacy because they are characteristic components of these plants. However, there are few scientific reports on the structural specificity and bioactivity evaluation of 5-methylcoumarin meroterpenoids.

Gerbera piloselloides (L.) Cass. is a perennial herb of the *Gerbera* genus (*sensu lato*), belonging to the subfamily Mutisioideae of Compositae. It is commonly distributed in the Yunnan, Guangxi, and Tibet provinces in southwest China¹³. The whole plant of *G. piloselloides* has been used as a folk medicine for the treatment of fever, cough, and snake bites, as well as a culinary spice for the improvement of flavour^{14–15}. In our ongoing search for structurally unique and biologically potent 5-methylcoumarin meroterpenoids from *G. piloselloides*¹⁶, (±)-gerbeloids A (**1**) featuring a unique caged oxatricyclo [4.2.2.0^{3,8}] decene framework, were isolated from this species (Fig. 1). Chiral separation and X-ray analysis led to the assignment of each optically pure enantiomer as (+)-**1a**, (–)-**1b**. The biomimetic synthesis of racemic **1** was achieved under the guidance of the hypothetical biosynthetic pathway. Subsequently, we evaluated the lipid-lowering activity *in vitro* using a model of 3T3-L1 adipocytes and *in vivo* using a model of high-fat diet zebrafish, thereby elucidating its anti-obesity effects and potential molecular mechanism of action.

Herein, we described the isolation, structural elucidation, chiral separation, hypothetical biogenetic pathway, and biomimetic synthesis, as well as the pharmacological activity study *in vitro* and *in vivo*.

2. Results and discussion

2.1. Structure elucidation

Gerbeloid A (**1**) was obtained as a white amorphous powder. Its molecular formula, C₂₀H₂₂O₃, with 10 degrees of unsaturation, was determined based on a quasi-molecular ion at *m/z* 311.1638 [M + H]⁺ (calcd for C₂₀H₂₃O₃⁺, 311.1642) in its HRESIMS (Supporting Information Fig. S7) and supported by its NMR data. The IR spectrum implied the existence of carbonyl groups (1748 cm^{–1}) and aromatic rings (1463 cm^{–1}). The ¹H and ¹³C NMR spectra (Supporting Information Figs. S8–S9) of **1** displayed the signals for an ester carbonyl (δ_C 167.4), four methyls [δ_H 2.47, 1.30, 1.09 and 1.13 (each 3H, s); δ_C 19.9, 27.8, 27.8 and 21.2], a set of the *cis* olefinic bond [δ_H 5.97 and 6.35 (each 1H, d, *J* = 10.8 Hz); δ_C 134.3 and 126.2] and a 1, 2, 3-trisubstituted benzene ring [δ_H 7.00 (1H, d, *J* = 7.6 Hz), 7.20 (1H, dd, *J* = 7.6, 8.2 Hz), and 6.87 (1H, d, *J* = 8.2 Hz); δ_C 124.1, 138.5, 128.1, 129.7, 115.2 and 151.1]. Comprehensive analysis (Fig. 2A) of ¹H–¹H COSY, HSQC, and HMBC spectra (Supporting Information Figs. S10–S12) of **1** resulted in the unambiguous assignment of its ¹H and ¹³C NMR signals as shown in Table 1. The ¹H–¹H COSY correlations of H-6/H-7/H-8, and HMBC correlations from H₃-16 to C-5/C-4a, and from H-7 to C-5/C-8a, together with two quaternary carbons C-4 (δ_C 69.7) and C-3 (δ_C 49.5) and the carbonyl carbon C-2 (δ_C 167.4) implied the presence of a 5-methylcoumarin moiety (subunits A and B in Fig. 1). Additionally, these data accounted for 7

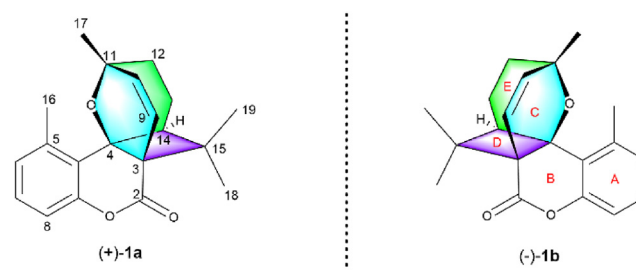


Figure 1 Structures of (±)-gerbeloid A [(±)-**1**].

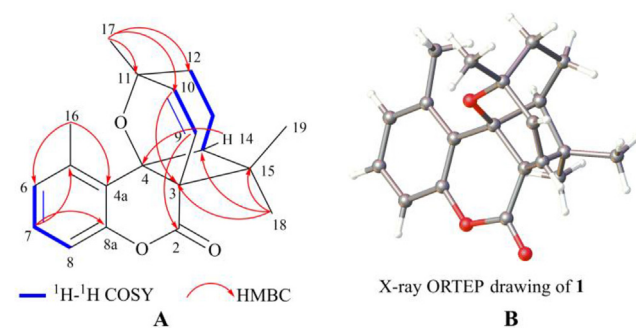


Figure 2 The Key ¹H–¹H COSY and HMBC correlations (A) and X-ray ORTEP drawing of **1** (B).

Table 1 ^1H (600 MHz) and ^{13}C (150 MHz) NMR data of **1** in CDCl_3 .

No.	1 (1a and 1b)		No.	1 (1a and 1b)	
	δ_{H} (multi, J in Hz)	δ_{C}		δ_{H} (multi, J in Hz)	δ_{C}
2	—	167.4	10	5.97 d (10.8)	134.3
3	—	49.5	11	—	69.9
4	—	69.7	12	1.65 ddd (13.2, 8.4, 1.2), 1.84 ddd (13.2, 11.4, 7.8)	30.1
4a	—	124.1	13	1.92 dddd (15.0, 11.4, 8.4, 4.8), 2.06 dddd (15.0, 12.0, 7.8, 1.2)	18.3
5	—	138.5	14	2.39 dd (12.0, 4.8)	43.2
6	7.00 d (7.6)	128.1	15	—	45.0
7	7.20 dd (7.6, 8.2)	129.7	16	2.47 s	19.9
8	6.87 d (8.2)	115.2	17	1.30 s	27.8
8a	—	151.1	18	1.09 s	27.8
9	6.35 d (10.8)	126.2	19	1.13 s	21.2

degrees of unsaturation and thus required three additional rings in the molecule. Further analysis of the HMBC correlations from H₃-17 to C-10/C-11, from H-10 to C-3, and from H-9 to C-2, as well as ^1H - ^1H COSY correlations of H-9/H-10 indicated the presence of a 6-methyl-3,6-dihydro-2H-pyran moiety (subunit C in Fig. 1), which was fused to the ring B to form the pyrano [3,2-*c*] coumarin core skeleton. Besides, the HMBC correlations from H₃-18 and H₃-19 to C-3/C-14/C-15, and from H-14 to C-4 revealed the dimethylated cyclobutane ring system (subunit D in Fig. 1), which fused to both rings B and C sharing the same bridgehead carbons C-3 and C-4. The ^1H - ^1H COSY correlations of H-12/H-13/H-14 and a key HMBC correlation between H₃-17 and C-12 established another new system of pyran ring (subunit E in Fig. 1), which fused with rings C and D *via* the bridgehead carbons C-4, C-11 and C-14. Therefore, the planar structure of **1** was established as shown in Fig. 1.

To validate the proposed structure described above and to solve the challenging stereochemistry of the hydrogen-free sp^3 carbons, which could not be determined by NMR methods (Supporting Information Fig. S13), we attempted to culture the single crystal of **1** in various conditions. Fortunately, after repeated attempts, single crystals of **1** were obtained in a solvent system of dichloromethane/methanol (2:1) at a constant temperature of 4 °C. The single crystal X-ray diffraction of **1** using Cu K α radiation confirmed the proposed planar structure and the relative configuration (Fig. 2B). However, the existence of a centrosymmetric space group $P2_12_12_1$ and large flack parameter values in the crystal structure, combined with its barely measurable optical rotation value, indicated that **1** was a racemic mixture. Subsequently, a pair of optically pure enantiomers, (+)-**1a** and (–)-**1b**, were successfully separated by chiral high-performance liquid chromatography (Supporting Information Figs. S1–S3), also proved by the respective specific rotation ($[\alpha]_{\text{D}}^{20} + 69.0$ and $[\alpha]_{\text{D}}^{20} - 60.0$) and opposite ECD curves (Fig. 3A). Finally, the X-ray crystallographic analyses [flack parameters: –0.12 (13) and –0.05 (8)] established unambiguously the absolute configurations of (+)-**1a** and (–)-**1b** to be 3*S*/4*R*/11*R*/14*S*, and 3*R*/4*S*/11*S*/14*R*, respectively (Fig. 3B and C).

2.2. Plausible biosynthetic pathway

Plausible biogenetic pathway for **1** is postulated in Scheme 1. Acetyl-CoA and malonyl-CoA, two common biosynthetic precursors of coumarins, were presumed to be the precursors for these metabolites. The 4-hydroxy-5-methylcoumarin (**2**), which is prevalent in the genus *Gerbera*, is synthesized from one

acetyl-CoA and four malonyl-CoAs through the polyketide pathway in plants⁷. Inspired by the biosynthetic pathway of tetrahydrocannabinolic acid in *Cannabis sativa*, we suggest that geranyl diphosphate (GPP) may first be introduced to C-3 of the coumarin skeleton as a monoterpene chain to form the prenylated intermediate **3**, which was subsequently oxidized to give **4**^{10,17}. Intermediate **4** is a flat ring without a chiral center, so we speculate that it can freely undergo oxa-6 π electrocyclicization in any direction of the molecular plane to form racemic mixture **5**, which is mutisicoumarin B (Supporting Information Figs. S14–S15) that we previously isolated from the same plant¹⁸. Intermediate **5** has one chiral center, and its three rings (A-B-C) are in the same plane because the benzene (A) ring forms a conjugated system with the double bonds in the B and C rings. For the *R*-intermediate of **5**, if 17-CH₃ is of β -configuration, then the flexible chain is of α -configuration. Thus, the olefinic bond at C-14/C-15 in the flexible chain can only be [2 + 2] cycloaddition with the olefinic bond at C-4/C-3 from the in-plane direction of the molecular plane to produce **1a**, and the same is for the *S*-intermediate of **5** (**1b**). That is the hypothetical biosynthetic pathway that produces racemic mixture **1** (Scheme 1).

2.3. Biomimetic synthesis of racemic **1**

The fascinating carbon skeleton of this coumarin-derived meroterpenoid and its significant bioactivities prompted us to conduct the biomimetic synthesis. Thus, guided by the hypothetical biosynthetic pathway, **1** was successfully synthesized over the two steps with 4-hydroxy-5-methylcoumarin and citral as the starting material. According to the previously reported method with a slight modification¹⁹, the key intermediate **5** (Supporting Information Figs. S18–S19) was obtained smoothly catalyzed by the phosphoric acid **6** through oxa-6 π -electrocyclization. The intermediate **5** is a racemic mixture composed of *R*-configuration and *S*-configuration in a ratio of 1:1 (Supporting Information Fig. S4). Then the irradiation of the intermediate **5** led to the formation of racemic **1** *via* intramolecular [2 + 2] photocycloaddition (Scheme 2, Supporting Information Figs. S16–S17). The effects of solvents on [2 + 2] cycloaddition were investigated. It turned out that the polar solvent was a suitable choice for the reaction and methanol provided the best result (Table 2). Notably, gerberoid 11 (compound **7**, Supporting Information Figs. S20–S21), which is a known natural product that we previously isolated from the same plant²⁰, was also obtained by [2 + 2] photocycloaddition with a 30% yield in methanol.

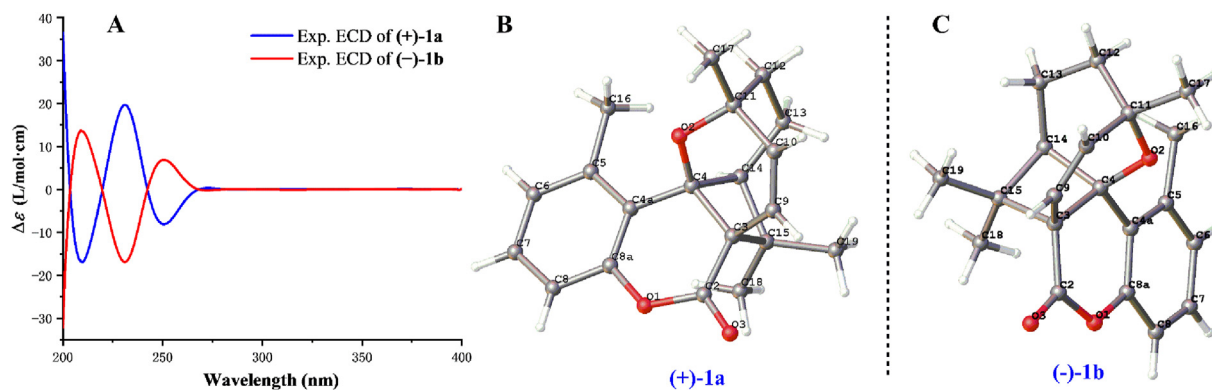


Figure 3 Experimental ECD spectra for compounds (+)-**1a** and (-)-**1b** (A); X-ray ORTEP drawing of (+)-**1a** (B); X-ray ORTEP drawing of (-)-**1b** (C).

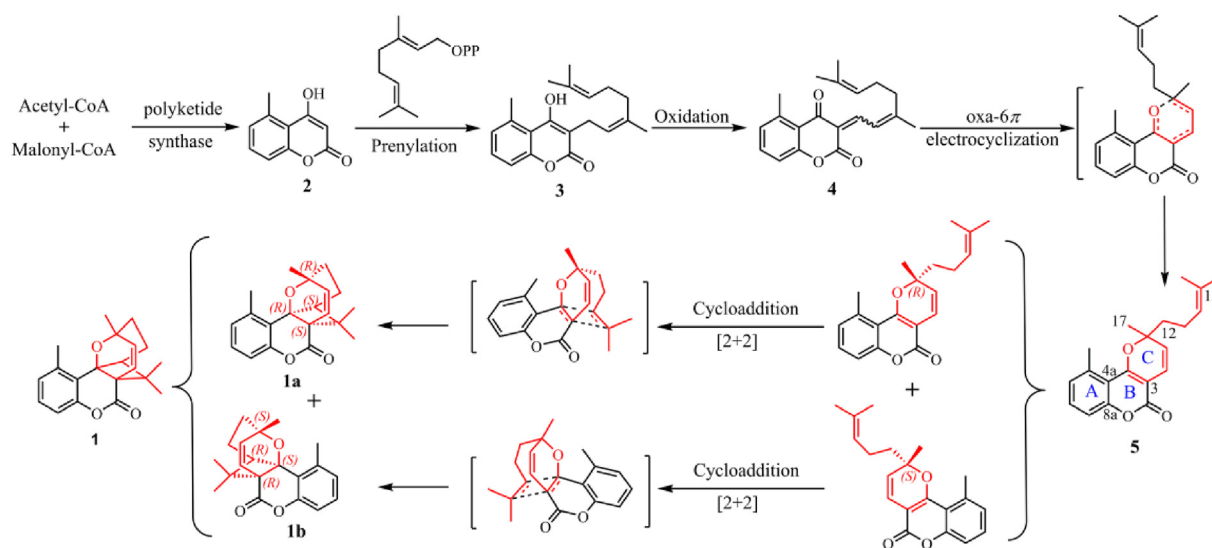
2.4. Evaluation of lipid-lowering activity of **1a/1b** *in vitro*

The 3T3-L1 mouse preadipocyte cell line has been widely used in obesity-related research and has the potential to differentiate from fibroblasts into adipocytes^{21–22}. Therefore, the 3T3-L1 adipocytes model (Fig. 4A) was used to evaluate the lipid-lowering efficacies of all the isolated compounds *in vitro* in this study. We initially observed the lipid-lowering effects of racemic mixtures **1**, **5**, and **7**, and found that only **1** reduced the number of lipid droplets and lipid accumulation at a concentration of 50 $\mu\text{mol/L}$, leading us to explore the anti-obesity efficacy of pure optical monomer (+)-**1a** and (-)-**1b** (Supporting Information Fig. S22). Firstly, none of (+)-**1a** nor (-)-**1b** showed any significant inhibition on the viability of the cultured 3T3-L1 cells at the concentrations tested (Fig. 4B). To observe the effects of (+)-**1a** and (-)-**1b** on adipocyte differentiation, levels of intracellular lipid droplets were visualized by the oil red o staining on differentiation Day 6. The results showed that both (+)-**1a** and (-)-**1b** reduced the number of lipid droplets and lipid accumulation in a dose-dependent manner, displaying potent lipid-lowering activity (Fig. 4C and D). Notably,

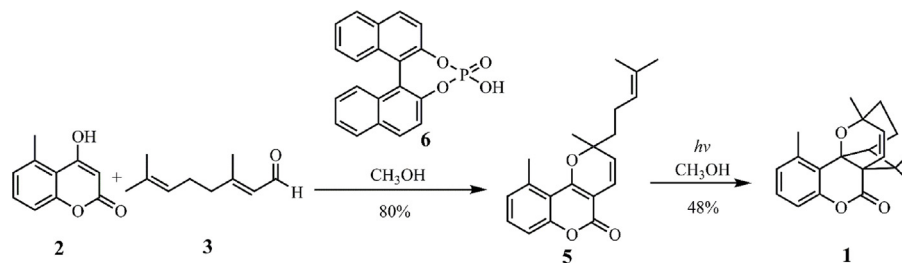
the lipid-lowering effect of (+)-**1a** was better than that of (-)-**1b** at the same concentration. Triglyceride (TG) content and glycerol-3-phosphate dehydrogenase (GPDH) activity were measured by using colorimetric kits, which are notable physiological markers of adipocyte differentiation and lipid biosynthesis. The results showed that both (+)-**1a** and (-)-**1b** markedly decreased TG content in a dose-dependent manner in 3T3-L1 cells on Day 6 of differentiation. Specifically, (+)-**1a** and (-)-**1b** at a concentration of 50 $\mu\text{mol/L}$ caused a 9.81- and 1.88-fold reduction of TG content compared to the IDIR group (Fig. 4E). Additionally, compared to the IDIR group, (+)-**1a** and (-)-**1b** reduced the activity of GPDH to 5.71- and 3-fold at a concentration of 50 $\mu\text{mol/L}$, respectively (Fig. 4F). These results indicate that (+)-**1a** and (-)-**1b** can act on adipocyte differentiation and in lipid storage in mature adipocytes, reversing lipid accumulation.

2.5. Evaluation of lipid-lowering activity of **1a/1b** *in vivo*

Zebrafish has emerged as an increasing disease model and is widely applied in the research of obesity, diabetes, and lipid



Scheme 1 Plausible biosynthetic pathway of **1**.



Scheme 2 Biomimetic synthesis of **1**.

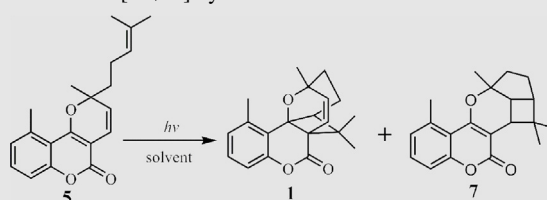
metabolism due to its characteristics of having 87% genome similarity with humans^{23–24}. Therefore, our study further used the high-fat diet (HFD) zebrafish model (Fig. 5B) to verify the lipid-lowering efficacies of (+)-**1a** and (–)-**1b** *in vivo*. The acute toxicity of (+)-**1a** and (–)-**1b** on 7 day-post-fertilization (dpf) zebrafish was assessed first, and (+)-**1a** and (–)-**1b** could induce lethal effects in a dose-dependent manner, the survival rates of (+)-**1a** and (–)-**1b** were gradually decreased above the exposure of 15 $\mu\text{mol/L}$, with non-lethal dose (LC_0) of 9.0 and 11.6 $\mu\text{mol/L}$, respectively (Fig. 5A). The effects of (+)-**1a** and (–)-**1b** with exposure of non-lethal dose in regulating lipid were measured by oil red o staining, which is a neutral lipid dye that can label the lipid droplets and dye it with a red color. As the results of oil red o staining shown (Fig. 5C), the red lipid droplet accumulation area within the model group increased gradually in the whole trunk and liver over time by the HFD zebrafish model compared with the control. However, the increase in red intensity and area were reversed by (+)-**1a** and (–)-**1b** (Fig. 5C), respectively. Furthermore, the contents of TG and total cholesterol (TC) of zebrafish were also measured. The reduction of (+)-**1a** was slightly better than (–)-**1b** at the exposure of high dose on the content of TG (1.99-fold for (+)-**1a**, and 1.94-fold for (–)-**1b**) and TC (1.59-fold for (+)-**1a**, and 1.46-fold for (–)-**1b**), compared to model (Fig. 5D and E). Taken together, our results validate the promising lipid-lowering effects of (+)-**1a** and (–)-**1b** *in vitro* and *in vivo*.

Furthermore, both *in vivo* and *in vitro*, the lipid-lowering effect of (+)-**1a** is superior to that of (–)-**1b**.

2.6. Study on the lipid-lowering mechanism of **1a/1b** *in vivo*

To investigate the mechanism by which (+)-**1a** and (–)-**1b** affected lipid accumulation, we examined the expression levels of genes involved in adipocyte differentiation and stimulating lipolysis. We initially detected the expression of the adipocyte differentiation-related genes *Pparg* and *Cebpa*. They are recognized as crucial adipogenic transcription factors that govern the promoters of downstream genes related to adipogenesis, thereby initiating the complete differentiation process necessary for adipocyte maturation^{25–26}. Reverse transcription-polymerase chain reaction (RT-PCR) analysis revealed that administration of **1a/1b** dramatically down-regulated the expressions of *Pparg* and *Cebpa* compared with the HFD zebrafish model group (Fig. 5F and G). Moreover, we also detected the mRNA levels of *Perilipin*, a key regulator that promotes lipolysis in adipose tissue. Our results showed that the expression levels of *Perilipin* significantly reduced in a roughly dose-dependent manner after treatment of (+)-**1a** and (–)-**1b** (Fig. 5H), suggesting that both (+)-**1a** and (–)-**1b** induced the constant lipolysis of adipocytes^{27–28}. The data suggest that (+)-**1a** and (–)-**1b** may

Table 2 The effects of solvents from **5** to **1** on [2 + 2] cycloaddition.



Entry	Solvent	Yield ^a	
		1	7
A	CH ₂ Cl ₂	12%	n.d. ^b
B	CH ₃ OH	48%	30%
C	EtOAc	10%	n.d.
D	THF	26%	n.d.
E	CH ₃ CH ₂ OH	28%	n.d.

^aYield of isolated product.

^bNot detected.

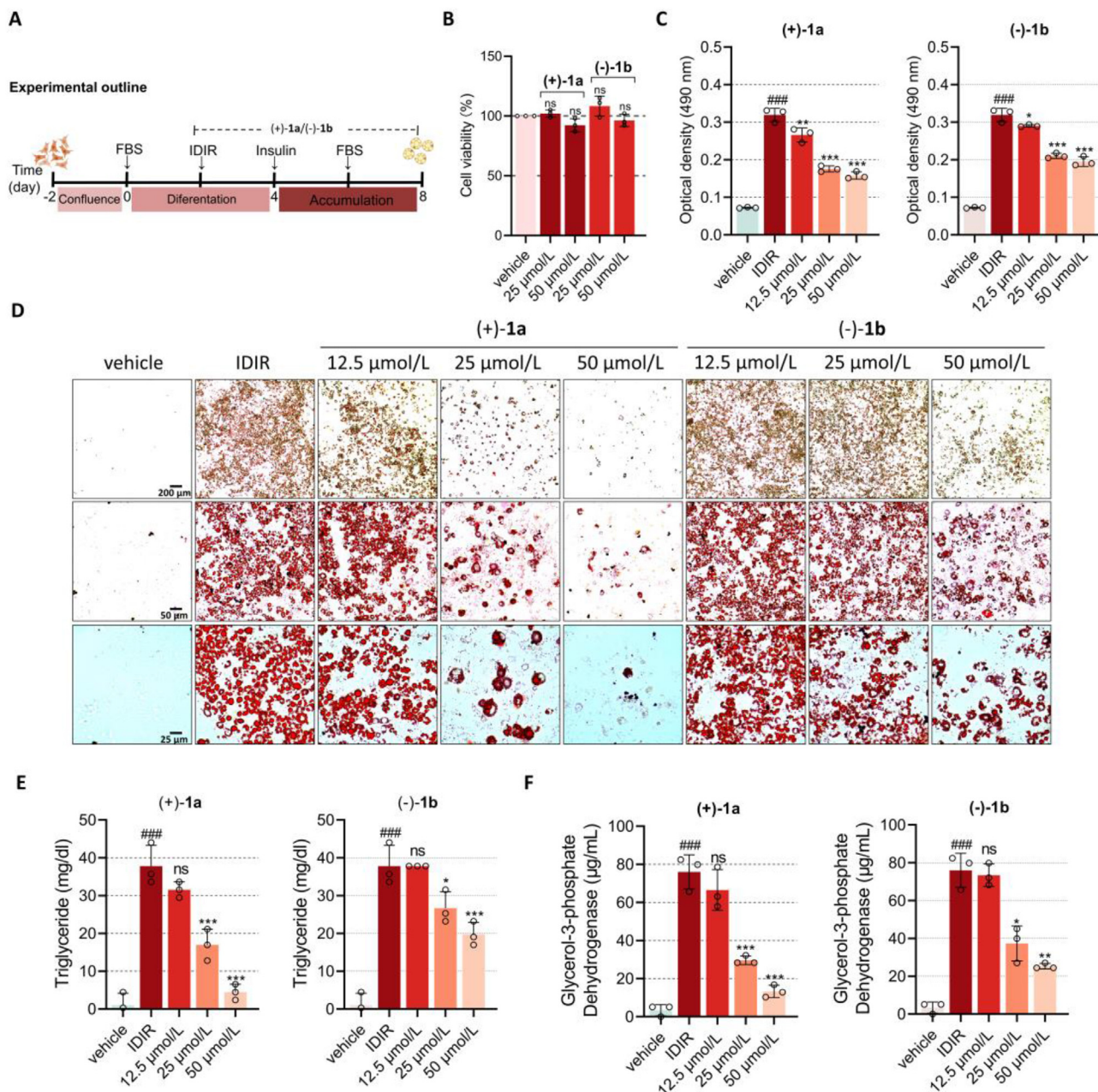


Figure 4 (+)-1a and (-)-1b inhibited adipogenic differentiation and lipid accumulation in 3T3-L1 adipocytes. (A) Experimental outline of mouse 3T3-L1 fibroblasts differentiated with IDIR induction medium. (B) The cell viability was determined by CCK-8 assay. (C) Adipocytes were stained with oil red o and quantified absorbance at 490 nm. (D) Adipocytes were stained with oil red o and visualized under microscopy, scale bar, 200, 50, 25 μm . (E) Adipocyte differentiation and lipid accumulation were accessed by TG content measurement and (F) GPDH content was determined by manual methods. The data are expressed as mean \pm SD ($n = 3$). ### $P < 0.001$ vs vehicle, ns $P > 0.05$, * $P < 0.05$, ** $P < 0.01$, *** $P < 0.001$ vs IDIR.

exert lipid-lowering effects by inhibiting adipocyte differentiation and stimulating lipolysis.

2.7. Mechanism exploration of 1a/1b involved in adipogenesis and lipolysis

The impacts of (+)-1a and (-)-1b on down-regulation of the gene expression of *Pparg*, *Cebpa*, and *Perilipin* prompted us to further investigate how (+)-1a and (-)-1b influence adipogenesis and lipolysis. Generally, CCAAT/enhancer binding proteins α (C/EBP α)

and peroxisome proliferator-activated receptor γ (PPAR γ) are the key transcription factors in the process of pre-adipocyte differentiation into adipocytes and lipogenesis²⁹. Western blot analysis revealed that IDIR-induced adipocytes differentiation was associated with significant increases in the expression of PPAR γ and C/EBP α , and (+)-1a and (-)-1b reduced the expression of PPAR γ and C/EBP α in differentiated 3T3-L1 adipocytes (Fig. 6A), suggesting that alteration of adipocyte differentiation in 3T3-L1 cells by (+)-1a and (-)-1b was associated with the regulation of C/EBP α /PPAR γ signaling. Moreover, the balance between lipid biosynthesis and lipolysis plays

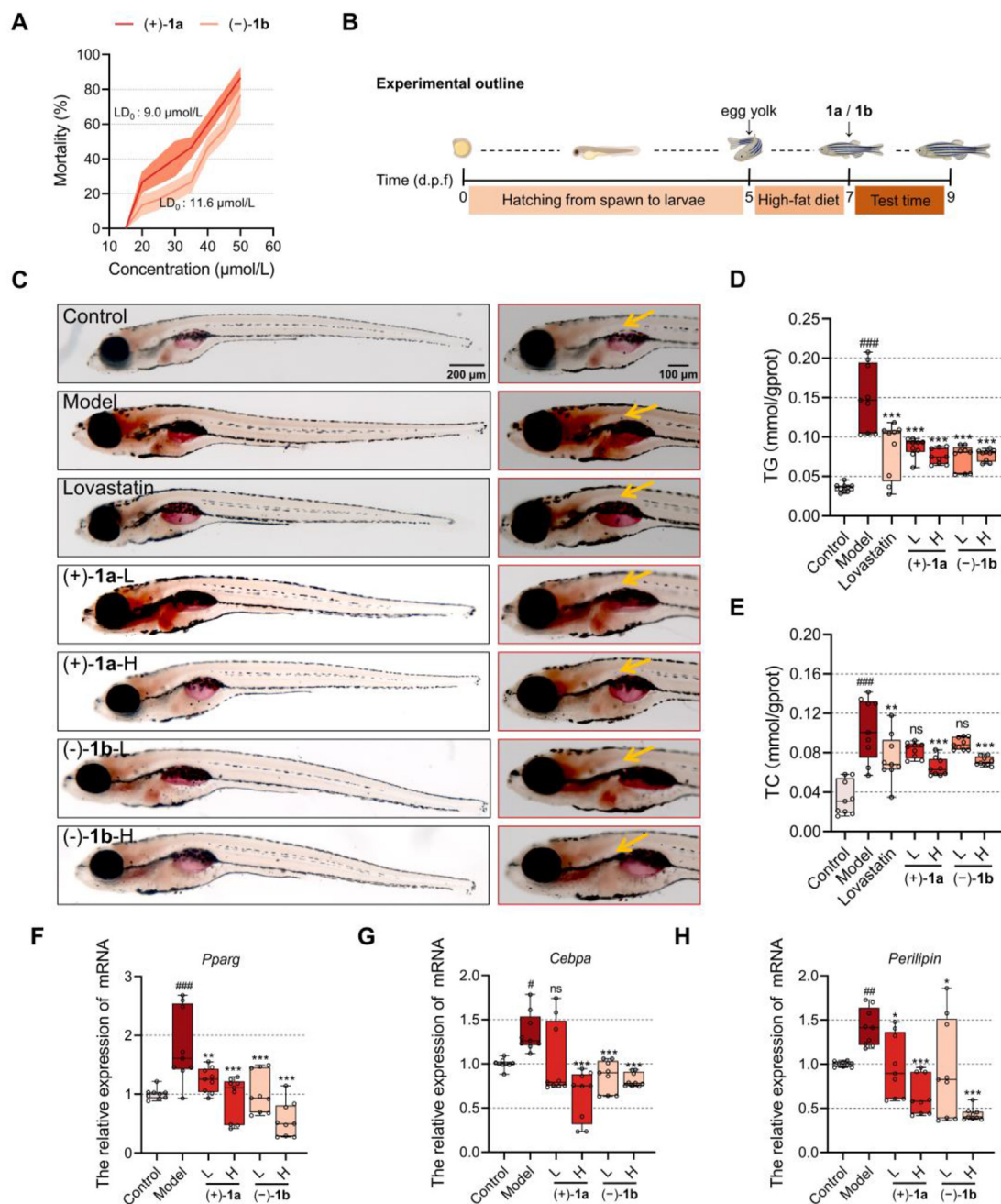


Figure 5 (+)-1a and (-)-1b exert a lipid-lowering effect on HFD zebrafish. (A) Dose-toxicity curve of (+)-1a and (-)-1b on 5 dpf zebrafish. (B) Experimental outline of HFD zebrafish with (+)-1a and (-)-1b treatment. (C) Zebrafish stained with oil red o and visualized under a microscope, Lovastatin, positive control at 2.0 $\mu\text{g/mL}$, scale bar, 200, 100 μm . (D) TG measurement and (E)TC content were determined by manual methods, Lovastatin, positive control at 2.0 $\mu\text{g/mL}$. (F) The effects of (+)-1a and (-)-1b on relative mRNA expression level of *Pparg*. (G) The effects of (+)-1a and (-)-1b on relative mRNA expression level of *Cebpa*. (H) The effects of (+)-1a and (-)-1b on relative mRNA expression level of *Perilipin*. The data are expressed as mean \pm SD ($n = 10$). ### $P < 0.001$ vs vehicle, $^{ns}P > 0.05$, * $P < 0.05$, ** $P < 0.01$, *** $P < 0.001$ vs Model. L: low concentration; H: high concentration.

a major role in regulating lipolysis in adipocytes pathway³⁰. PKA-mediated lipolysis signaling is an important mechanism to reverse lipid accumulation, and involves the phosphorylation of protein kinase A (PKA) on oil globules, resulting in lipolysis by activation of hormone-sensitive lipase (HSL) and phosphorylated HSL at Ser660/Ser563³¹. Perilipin, the most abundant protein-coated lipid droplets in adipocytes, phosphorylated HSL is transferred from the cytoplasm to the surface of the lipid droplet, consequently hydrolyzing TG^{32–33}.

As shown in Fig. 4D, treatments with (+)-1a and (-)-1b led to the degradation of lipid droplets, and the lipid droplets became much smaller. Then we further confirmed the effects of (+)-1a and (-)-1b on the expression of lipolytic regulators. Western blot analysis showed that (+)-1a and (-)-1b increased the expression of the p-PKA and p-HSL₅₆₃/p-HSL₆₆₀. Additionally, both (+)-1a and (-)-1b significantly decreased the expression of perilipin in 3T3-L1 adipocytes. These findings suggest that the alteration of adipocyte

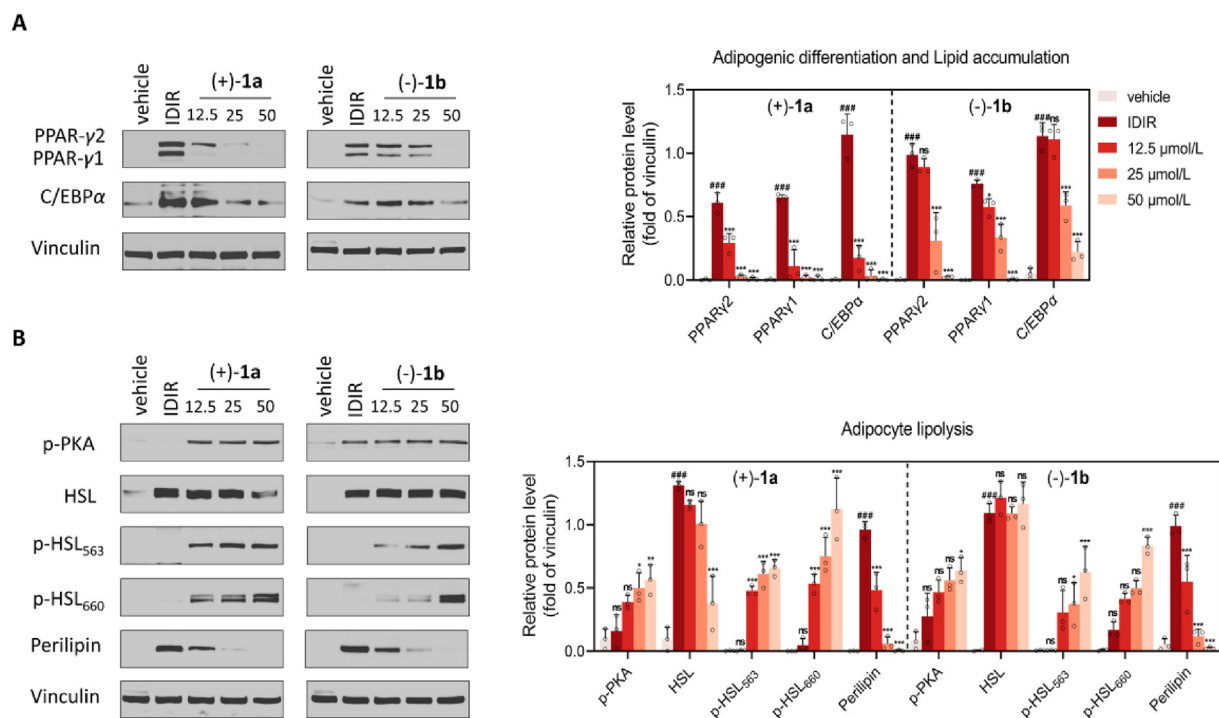


Figure 6 (+)-**1a** and (-)-**1b** regulated the expression of adipogenic and lipogenic proteins in 3T3-L1 adipocytes. The 3T3-L1 adipocytes were incubated with a control vehicle or (+)-**1a** and (-)-**1b** (12.5, 25, and 50 $\mu\text{mol/L}$) for 6 days. (A) Expression of proteins involved in adipogenic differentiation and lipid accumulation (PPAR γ and C/EBP α) was determined by Western blot, vinculin was used as a loading control. (B) Expression of proteins involved in adipocyte lipolysis (p-PKA, HSL, p-HSL₅₆₃, p-HSL₆₆₀, and Perilipin) was detected by Western blot, vinculin was used as a loading control. The data are expressed as mean \pm SD ($n = 3$). #### $P < 0.001$ vs vehicle, ^{ns} $P > 0.05$, * $P < 0.05$, ** $P < 0.01$, *** $P < 0.001$ vs IDIR.

lipolysis in 3T3-L1 adipocytes by (+)-**1a** and (-)-**1b** were associated with the cascade regulation of PKA signaling (Fig. 6B). Taken together, our study proposes that the regulation of C/EBP α /PPAR γ signaling and Perilipin-mediated signaling by (+)-**1a** and (-)-**1b** impairs adipocytes differentiation and stimulates lipolysis in 3T3-L1 adipocytes and high-fat diet zebrafish.

3. Conclusions

In summary, a pair of new skeleton natural products (\pm)-gerbeloid A were isolated from the medicinal plant *G. piloselloides*. Their structures were exhaustively characterized by comprehensive spectroscopic data and X-ray diffraction analysis. Biosynthetically, **1** is extremely unprecedented for the C-3/C-4 double bond of natural coumarin meroterpenoids to be involved in intramolecular [2 + 2] ring addition. The highly structural novelty and potent biological activity of **1** prompted us to chemically synthesize from commercially available materials *via* a linear strategy, resulting in **1** (target product), **5** (intermediate product), and **7** (by-product). Structurally, **1** exhibits more fascinating three-dimensional structural features compared to the plane character of **5** and **7**. From the perspective of the three olefin double bonds in intermediate product **5** that participated in the biosynthetic reaction, we speculate that multiple byproducts with novel scaffolds remain to be explored. Importantly, we not only established the synthesis route of 5-methylcoumarin meroterpenoids for the first time based on the plausible biosynthetic pathways but also provided a sustainable source for further bioactive evaluation.

Using a model of 3T3-L1 adipocytes and high-fat diet zebrafish, it was found that both (+)-**1a** and (-)-**1b** exhibited potent lipid-lowering activity *in vitro* and *in vivo*. The molecular mechanism studies have shown that (+)-**1a** and (-)-**1b** impair adipocyte differentiation and stimulate lipolysis by regulating C/EBP α /PPAR γ signaling and Perilipin signaling. In particular, we can speculate that (+)-**1a** and (-)-**1b** exhibit superior or equal lipid-lowering activity compared to positive control metformin (a plant-derived clinical drug) and lovastatin (a synthetic clinical drug) based on the limited bioactivity data. Taking together the outcomes of bioactivity and mechanism as well as unprecedented structural features, a unique caged oxatricyclo [4.2.2.0^{3,8}] decene motif of **1** may be an effective group for lipid-lowering effects. Therefore, our findings not only provide chemists with novel structural templates and synthetic routes but also provide candidate molecules for the discovery of innovative anti-obesity drugs.

4. Experimental

4.1. General experimental procedures

Optical rotations were obtained on an Anton Paar MCP 200 Automatic Polarimeter (Anton Paar GmbH, Graz, Austria). IR and UV spectra were recorded on a Nicolet IS5 FT-IR spectrophotometer (Thermo Scientific, Madison, WI, USA) and a Thermo Genesis-10S UV-Vis spectrophotometer (Thermo Scientific, Madison, WI, USA), respectively. ECD spectra were acquired on an Applied

Photophysics Chirascan spectropolarimeter (Applied Photophysics Ltd., Leatherhead, UK). The HRESIMS spectra were recorded using the Q-TOF analyzer of a SYNAPT HDMS system (Waters, Milford, MA, USA). ^1H and ^{13}C NMR data were acquired with Bruker 600 instruments (Bruker, Rheinstetten, Germany) using the solvent signals (CDCl_3 : δ_{H} : 7.26/ δ_{C} : 77.16 ppm) as references. HPLC system used for purification included a 2535 instrument equipped with a 2489 UV detector (Waters, USA). Silica gel (60–100, 100–200, 200–300 mesh) was supplied by Qingdao Marine Chemical Plant (Qingdao, China). Chiral column employed was Chiralpak[®]IA (0.46 cm \times 25 cm, i.d., 10 μm) and Chiralpak[®]IBN-5 column (0.46 cm \times 25 cm, i.d., 5 μm) (Daicel corporation, Japan). Single crystal data were collected using a Gemini E X-ray single crystal diffractometer with a graphite monochromated Cu K α radiation (Agilent, Britain). Fetal bovine serum (10099-141), Dulbecco's modified Eagle medium (8122175), Pen-streptomycin (15140-122), Typsin-EDTA (25200072) were purchased from Gibco (Cambridge, USA); Anti-PKA (ab75991) was purchased from Abcam (Cambridge, UK); PPAR γ (2435T), C/EBP α (8178T), Vinculin (13901S) and Lipolysis activation antibody sampler kit (8334T) were purchased from Cell signaling technology (Danvers, USA). TG assay kit was purchased from Cayman Chemical (Ann Arbor, USA). GPDH assay kit was purchased from Sciencell (Carlsbad, USA). The modified oil red o staining kit was purchased from Beyotime (Shanghai, China). TC assay kit and TG assay kit were purchased from Nanjing Jiancheng Bioengineering Institute (Nanjing, China). Egg yolk powder was purchased from Yuanye (Shanghai, China). The total RNA was extracted from larval zebrafish using the TRIzol reagent (LABLEAD, 1000012721, China). The reverse transcription was performed using the First-Strand Synthesis MasterMix cDNA synthesis (LABLEAD, 0202120731, China). The gene expression level was evaluated using an ABI Step One plus RT-PCR system (Applied Biosystem, USA) with 2 \times Realab Green PCR Fast mixture (LABLEAD, 0202102731, China). Unless otherwise noted, all chemicals were obtained from commercially available sources and were used without further purification.

4.2. Plant material

The air-dried whole plants of *G. piloselloides* (L.) Cass. (Compositae) were collected from Yulin City, Guangxi province, China (GPS coordinates: 21° 55' 14.71" N, 110° 16' 3.60" E; Altitude: 800 m), in November 2019 and authenticated by professor Yun-Feng Huang (Institute of Chinese Medicine Resources, Guangxi Institute of Chinese Medicine & Pharmaceutical Science, Nanning, China). A voucher specimen (SCI-NCL006379-1) was deposited in the National Compounds Library of Traditional Chinese Medicines (NCL-TCM), Institute of Medicinal Plant Development (IMPLAD), Chinese Academy of Medical Sciences and Peking Union Medical College (CAMS & PUMC), China.

4.3. Extraction and isolation

The air-dried whole plants of *G. piloselloides* (30 kg) were powdered and extracted with 95% EtOH (300 L \times 2 h \times 2 times) under heating and refluxing. The EtOH extract was concentrated under reduced pressure to yield a brown residue (2.1 kg), which was suspended in H $_2$ O and partitioned in turn with petroleum ether (PE) (bp 60–90 °C), EtOAc, and *n*-BuOH, respectively. The petroleum ether extract (171 g) was subjected to column chromatography (CC) over silica gel using sequential gradient elution of PE/CH $_2$ Cl $_2$ (100:0 \rightarrow 0:100) to obtain three main fractions (Fr. A–Fr. C). Fr. C (18 g) was

fractionated into five subfractions (Fr. C1–Fr. C5) by silica gel chromatography (PE/CH $_2$ Cl $_2$ 10:0 \rightarrow 0:10). Fr. C4 (2.5 g) was purified by preparative HPLC (85% MeOH in H $_2$ O, 8 mL/min) to give six sub-subfractions (Fr. C4.1–Fr. C4.6), then Fr. C4.1 (69 mg) was purified by semi-preparative HPLC (75% MeOH in H $_2$ O, 2 mL/min) to afford **1** (3.5 mg, t_{R} = 29 min). **1** was further separated by chiral resolution to obtain compounds **1a** and **1b**.

4.4. Physical constants and spectral data

Gerbeloid A (**1**): Colourless crystal (CH $_2$ Cl $_2$ –MeOH); $[\alpha]_{\text{D}}^{20}$ 0 (c 0.1, MeOH); UV (CH $_3$ OH) λ_{max} (log ϵ): 215 (3.65), 269 (3.34), 283 (3.20) nm (Supporting Information Fig. S5); IR (neat) ν_{max} 2929, 1748, 1463, 1386, 1249, 1100, 1039, 822 cm $^{-1}$ (Supporting Information Fig. S6); ^1H and ^{13}C NMR data, see Table 1; HR-ESI-MS m/z 311.1638 [M + H] $^+$ (calcd for C $_{20}$ H $_{23}$ O $_3^+$, 311.1642).

(+)-Gerbeloid A (**1a**): colourless crystal (CH $_2$ Cl $_2$ –MeOH); $[\alpha]_{\text{D}}^{20}$ + 69.0 (c 0.1, MeOH); ECD (MeOH) λ_{max} ($\Delta\epsilon$) 210 (–16.95), 231 (+19.71), 251 (–8.13).

(–)-Gerbeloid A (**1b**): colourless crystal (CH $_2$ Cl $_2$ –MeOH); $[\alpha]_{\text{D}}^{20}$ – 60.0 (c 0.1, MeOH); ECD (MeOH) λ_{max} ($\Delta\epsilon$) 209 (+13.68), 231 (–16.93), 251 (+6.92).

4.5. X-ray crystallographic analysis

The crystals of **1** is orthorhombic (0.37 mm \times 0.26 mm \times 0.17 mm), obtained in a culture solvent of MeOH–CH $_2$ Cl $_2$ (1:2, *v/v*). Crystal data: C $_{20}$ H $_{22}$ O $_3$, M = 310.38, T = 110.3 (3) K, space group $P2_12_12_1$ (no.19). Cell parameters: a = 8.7901 (2) Å, b = 10.6031 (3) Å, c = 17.0299 (4) Å, α = 90°, β = 90°, γ = 90°, V = 1587.21 (7) Å 3 , Z = 4, ρ = 1.322 mg/mm 3 , μ (Cu K α) = 0.687 mm $^{-1}$; 7224 reflections measured, 3008 unique (R_{int} = 0.0269) which were used in all calculations. Final R indexes [$I > 2\sigma(I)$]: R_1 = 0.0363, and wR_2 = 0.0928; Final R indexes (all data): R_1 = 0.0378, and wR_2 = 0.0945. Flack parameters = 0.0 (5). Crystal data of **1** was deposited with the Cambridge Crystallographic Data Centre (CCDC 2079802).

The crystal of **1a** is orthorhombic (0.27 mm \times 0.26 mm \times 0.13 mm), obtained in a culture solvent of MeOH–CH $_2$ Cl $_2$ (1:2, *v/v*). Crystal data: C $_{20}$ H $_{22}$ O $_3$, M = 310.37, T = 113.8 (10) K, space group $P2_12_12_1$ (no.19). Cell parameters: a = 8.7902 (4) Å, b = 10.6042 (3) Å, c = 17.0295 (4) Å, α = 90°, β = 90°, γ = 90°, V = 1587.39 (9) Å 3 , Z = 4, ρ = 1.229 mg/mm 3 , μ (Cu K α) = 0.687 mm $^{-1}$; 5680 reflections measured, 3008 unique (R_{int} = 0.0290) which were used in all calculations. Final R indexes [$I > 2\sigma(I)$]: R_1 = 0.0376, and wR_2 = 0.0928; Final R indexes (all data): R_1 = 0.0395, and wR_2 = 0.0947. Flack parameters = –0.12 (13). Crystal data of compound **1a** was deposited with the Cambridge Crystallographic Data Centre (CCDC 2080074).

The crystal of **1b** is orthorhombic (0.29 mm \times 0.23 mm \times 0.14 mm), obtained in a culture solvent of MeOH–CH $_2$ Cl $_2$ (1:2, *v/v*). Crystal data: C $_{20}$ H $_{22}$ O $_3$, M = 310.37, T = 109.4 (7) K, space group $P2_12_12_1$ (no.19). Cell parameters: a = 8.79051 (14) Å, b = 10.60090 (17) Å, c = 17.0254 (3) Å, α = 90°, β = 90°, γ = 90°, V = 1586.55 (4) Å 3 , Z = 4, ρ = 1.299 mg/mm 3 , μ (Cu K α) = 0.687 mm $^{-1}$; 10,606 reflections measured, 3041 unique (R_{int} = 0.0346) which were used in all calculations. Final R indexes [$I > 2\sigma(I)$]: R_1 = 0.0376, and wR_2 = 0.0951; Final R indexes (all data): R_1 = 0.0377, and wR_2 = 0.0962. Flack parameters = –0.05 (8). Crystal data of compound **1b** was deposited with the Cambridge Crystallographic Data Centre (CCDC 2079804).

4.6. Biomimetic experimental procedures for compound **1**

4.6.1. The procedure for the preparation of **5**

To a solution of 4-hydroxy-5-methylcoumarin **2** (600 mg, 3.4 mmol) in CH₃OH (8 mL) was added citral **3** (1035 mg, 6.8 mmol) and the phosphoric acid **6** (60 mg, 0.17 mmol) at room temperature. After being stirred for 8 h, the solvent was evaporated under vacuum and the residue was purified by column chromatography (petroleum ether: ethyl acetate = 30:1) to give **5** (846 mg, Yield: 80%).

Compound **5**: Yield: 80%. ¹H NMR (600 MHz, Chloroform-*d*): δ 7.34 (dd, *J* = 8.3, 7.5 Hz, 1H), 7.14 (d, *J* = 8.3 Hz, 1H), 7.01 (d, *J* = 7.5 Hz, 1H), 6.57 (d, *J* = 10.1 Hz, 1H), 5.42 (d, *J* = 10.1 Hz, 1H), 5.09 (t, *J* = 7.1 Hz, 1H), 2.72 (s, 3H), 2.22–2.08 (m, 2H), 1.92 (ddd, *J* = 14.2, 10.9, 5.8 Hz, 1H), 1.74 (ddd, *J* = 14.2, 11.1, 5.2 Hz, 1H), 1.61 (s, 3H), 1.55 (s, 3H), 1.52 (s, 3H); ¹³C NMR (150 MHz, Chloroform-*d*): δ 162.0, 161.0, 154.5, 137.0, 132.5, 131.4, 127.5, 123.9, 123.4, 117.9, 115.4, 114.3, 100.2, 83.5, 41.9, 27.5, 25.7, 23.5, 23.1, 17.7.

4.6.2. The procedure for the preparation of **1**

A solution of **5** (200 mg, 0.32 mmol) in CH₃OH (5.0 mL) was irradiated with a 500 W high-pressure mercury lamp for 10 h. The solvent was evaporated under vacuum and the residue was purified by preparative thin-layer chromatography (CH₂Cl₂:CH₃OH = 50:1) to give compounds **1** and **7**.

Compound **1**: Yield: 48%. ¹H NMR (600 MHz, Chloroform-*d*): δ 7.20 (dd, *J* = 8.2, 7.6 Hz, 1H), 7.00 (d, *J* = 7.6 Hz, 1H), 6.87 (d, *J* = 8.2 Hz, 1H), 6.35 (d, *J* = 10.8 Hz, 1H), 5.97 (d, *J* = 10.8 Hz, 1H), 2.47 (s, 3H), 2.39 (dd, *J* = 12.0, 4.8 Hz, 1H), 2.09–2.02 (dddd, *J* = 15.0, 12.0, 7.8, 1.2 Hz, 1H), 1.96–1.88 (dddd, *J* = 15.0, 11.4, 8.4, 4.8 Hz, 1H), 1.84 (ddd, *J* = 13.2, 11.4, 7.8 Hz, 1H), 1.65 (ddd, *J* = 13.2, 8.4, 1.2 Hz, 1H), 1.30 (s, 3H), 1.13 (s, 3H), 1.08 (s, 3H); ¹³C NMR (150 MHz, Chloroform-*d*): δ 167.4, 151.1, 138.5, 134.3, 129.7, 128.2, 126.2, 124.0, 115.2, 69.9, 69.6, 49.4, 45.0, 43.1, 30.1, 27.8, 27.8, 21.2, 19.9, 18.3.

Compound **7**: Yield: 30%. ¹H-NMR (600 MHz, Chloroform-*d*): δ 7.00 (d, *J* = 7.4 Hz, 1H), 7.31 (dd, *J* = 8.2, 7.4 Hz, 1H), 7.16 (d, *J* = 8.2 Hz, 1H), 3.03 (d, *J* = 9.5 Hz, 1H), 2.66 (dd, *J* = 9.5, 7.5 Hz, 1H), 1.82 (m, 1H), 2.06 (m, 1H), 1.64 (m, 1H), 1.77 (1H, m, 1H), 2.45 (1H, t, *J* = 7.5 Hz, 1H), 2.71 (s, 3H), 1.52 (s, 3H), 1.42 (s, 3H), 0.88 (s, 3H); ¹³C-NMR (150 MHz, Chloroform-*d*): δ 163.2, 103.3, 161.6, 115.2, 136.8, 127.4, 130.5, 115.2, 154.0, 36.3, 37.7, 86.6, 39.7, 26.1, 47.0, 39.6, 23.7, 27.5, 33.9, 17.7.

4.7. Cell culture

The pre-adipose 3T3-L1 cells (mouse embryo fibroblast cell line) were maintained in Dulbecco's modified eagle medium (DMEM) supplemented with 10% (*v/v*) newborn calf serum, 100 U/mL penicillin and 100 µg/mL streptomycin at 37 °C in a humidified atmosphere with 5% CO₂. The cells were grown in 75 cm² culture flasks and were passaged strictly once they reached a density of 6 × 10⁴ viable cells/cm². To induce commitment, 3T3-L1 cells were seeded at 40%–50% confluence to reach full confluence on the following 2 days (Day –2 to Day 0). At 48 h post-confluence, cell differentiation was induced by changing the IDIR medium containing 10% fetal bovine serum, 0.5 mmol/L IBMX, 1 µmol/L dexamethasone, 10 µg/mL insulin, and 0.5 µmol/L rosiglitazone (Day 0 to Day 2). After 48 h, the medium was replenished with DMEM

containing 10% FBS and 10 µg/mL insulin for 48 h (Day 2 to Day 4). To stimulate lipid droplet accumulation, the differentiated cells were changed to DMEM containing 10% FBS for 48 h (Day 4 to Day 6). The differentiation process was observed. Intracellular lipid droplets started to appear on day 4 and continued to increase in both number and size in the subsequent days. The test compounds were initially added on Day 0 and regularly replenished throughout the entire culture period.

4.8. CCK-8 assay

Exponentially growing 3T3-L1 cells were seeded at 1 × 10⁴ cells per well in 96-well plates and incubated in a humidified cell incubator at 37 °C, 5% CO₂ for adherence. The cells were then treated with **1**, (+)-**1a**, and (–)-**1b** of 25, 50 µmol/L for 24 h, just after the completion of the incubation period, 10 µL CCK-8 reagents were then added, followed by an additional incubation for 1 h at 37 °C. After that, the optical density of plates was measured by a microplate reader (BioTek, Winooski, VT, USA) at the absorption values of 450 nm.

4.9. Oil red o staining assay

Differentiated 3T3-L1 adipocytes were fixed in 4% formaldehyde for 30 min at room temperature and washed twice with PBS. Oil red o staining was performed using the lipid staining kit according to the manufacturer's instructions. After staining, the cells were imaged under a confocal scanning microscope. For quantification analysis, oil red o staining was extracted with isopropanol and measured with a microplate reader at 490 nm.

4.10. TG assay

Differentiated 3T3-L1 adipocytes were washed twice with cold PBS and collected cells by a rubber policeman, the cells were lysed in lysis buffer and homogenized with sonication three times for 5 s at 20% amplitude followed by centrifugation at 12,000 × *g* for 20 min at 4 °C. The assay ran according to manufacturer instructions with a sample dilution of 1:5.

4.11. GPDH assay

Differentiated 3T3-L1 adipocytes were washed twice with cold PBS, cells were lysed in lysis buffer and sonicated three times for 5 s at 20% amplitude followed by centrifugation at 12,000 × *g* for 20 min at 4 °C, GPDH activity was assayed in the supernatants using GPDH Assay Kit.

4.12. Zebrafish breeding and modeling

The wild-type AB zebrafish used in this experiment were cultured and supplied by the Beijing Key Laboratory for Quality Evaluation of Chinese Materia Medica at the Beijing University of Chinese Medicine. The adult fish were raised in a centralized zebrafish circulating aquaculture system (Beijing Aisheng Technology Co., Ltd.). The circulating water system was maintained at 28 ± 0.5 °C, pH = 7.4, dissolved oxygen value is 7.5–8.0 mg/L, and the light control of the breeding room is alternately day (14 h) and night (10 h). Zebrafish embryos and larvae were cultured at 28 °C in embryo culture water (0.137 mol/L NaCl, 5.4 mol/L KCl, 0.25 mol/L disodium hydrogen phosphate, 0.44 mol/L K₂HPO₄, 1.3 mol/L CaCl₂, 1.0 mol/L MgSO₄, 4.2 mol/L NaHCO₃;

conductivity: 450–550 $\mu\text{S}/\text{cm}$; pH 7.0–8.0). To establish a high-fat diet model, zebrafish 5 days after fertilization were fed with 1.5% egg yolk for 48 h. All experiments were by the Animal Management Rules of the Ministry of Science and Technology of the People's Republic of China for experimental care and use of animals and approved by the Animal Ethics Committee of Beijing University of Traditional Chinese Medicine.

4.13. The acute toxicity and the maximum non-lethal dose (LC_0) evaluation

In total, zebrafish cultured to 7 dpf were selected and randomly divided into 9 groups with 10 zebrafish in each group including a blank control group, and 10 experiment groups (treated with different drugs at different dosages). zebrafish (7 dpf) were exposed to different concentrations (50, 45, 40, 35, 30, 25, 20, and 15 $\mu\text{mol}/\text{L}$) of (+)-**1a** and (–)-**1b** in 12-well plates with 10 zebrafish/well of 4 mL of test solution for 48 h. After 2 h, the phenotype and mortality of zebrafish were observed and recorded to determine the MTC, the dose-toxicity curve and LC_0 were calculated by GraphPad Prism 8.0 software.

4.14. Oil red o staining

The doses of (+)-**1a** and (–)-**1b** were set to 6, 9 $\mu\text{mol}/\text{L}$ (including 1/2 LC_0 and 3/5 LC_0) and 8, 12 $\mu\text{mol}/\text{L}$ (including 1/2 LC_0 and 3/5 LC_0) were selected as the subsequent experimental concentrations to investigate the lowing-lipid effect of (+)-**1a** and (–)-**1b**, respectively. Treatment was performed until 7 dpf with (+)-**1a** and (–)-**1b**. On the final day, the zebrafish were euthanized and fixed in paraformaldehyde (4%) overnight. The fixed zebrafish were washed in PBS, sequentially infiltrated with 50%, 75%, and 100% 1,2-propanediol for 10 min, then washed in PBS. Fresh oil red o solution (0.5%) was added to dye the zebrafish for 20 h, after which the zebrafish were washed with PBS. Stained larvae were stored in 100% glycerol and imaged by using a microscope.

4.15. TG and TC content assay

For measurement of TG and TC content, the zebrafish after exposure to (+)-**1a** and (–)-**1b** were harvested, zebrafish from each group were homogenized in 0.9% normal saline (1:9, v/v) and centrifuged at 2000 rpm for 15 min. The TG and TC levels were then determined according to the manufacturer's instructions.

4.16. RT-PCR

A total of 120 larvae were harvested after exposure to (+)-**1a** and (–)-**1b**, and their total RNA was extracted using TRIzol reagent. The quality of RNA was assessed by measuring the OD at 260 and 280 nm. Following reverse transcription to complementary DNA, the PCR system was utilized to quantify the mRNA expression levels of *Pparg*, *Cebpa*, and *Perilipin*. The PCR reaction conditions and volume adhered to the instructions provided in the kit. Each sample was analyzed in triplicate, and the relative gene expression was calculated using the $2^{-\Delta\Delta\text{CT}}$ method. The results are presented graphically in arbitrary units, indicating the ratio of the target gene to the internal reference gene (*Vinculin*). The primer sequences used in the study can be found in Supporting Information Table S1.

4.17. Western blot

3T3-L1 cells collected cells by a rubber policeman and lysed with precooled RIPA lysis buffer on ice for 30 min, and then the lysate was centrifuged at 12,000 rpm for 10 min at 4 °C. The protein concentration was quantified by the bicinchonic acid method, 20 μg of protein was loaded on the gel and separated by 8%–16% bis–tris PAGE, and the protein was transferred onto a PVDF membrane. Then, the membranes were blocked with western blocking buffer at room temperature for 1 h, incubated with primary antibodies at 4 °C overnight, and washed 4 times with Tris-buffered saline (TBST) containing Tween-20 buffer and incubated with horseradish peroxidase-linked secondary antibody for 1 h at room temperature. The membranes were washed 4 times with TBST, and the immunoreactive bands were visualized electrochemiluminescence (ECL) by a scanner.

4.18. Statistical analysis

The statistical analyses were performed with GraphPad Prism 8.0 software, and all data were presented as mean \pm SD. One-way ANOVA was applied to analyze the statistical differences among different groups, and $P < 0.05$ was taken as statistically significant.

Acknowledgments

We acknowledge financial support from the Natural Sciences Foundation of China (82374035), and the CAMS Innovation Fund for Medical Sciences (CIFMS, 2022-I2M-1-017, China).

Author contributions

Zhongmei Zou initiated and coordinated the project. Zhongmei Zou and Tao Zhang designed the experiments. Tao Zhang, Hai Shang, Chenxu Zhao, and Jingrong Li writing the original draft. Chenxu Zhao performed compound isolation and structure identification. Jingrong Li and Chenxu Zhao contributed to the bioactive study. Tao Zhang and Lingyu Li speculated on plausible biosynthetic pathways. Hai Shang and Yue Hu conducted the biomimetic synthesis experiment. Tao Zhang, Hai Shang, Meng Yu, Chenxu Zhao, and Jingrong Li analyzed the data. Yunfeng Huang identified the plant material. Zhongmei Zou performed manuscript revision. All authors approved the submitted version.

Conflicts of interest

The authors declare no conflicts of interest.

Appendix A. Supporting information

Supporting data to this article can be found online at <https://doi.org/10.1016/j.apsb.2024.03.035>.

References

1. Jin X, Qiu TT, Li L, Yu RL, Chen XG, Li CG, et al. Pathophysiology of obesity and its associated diseases. *Acta Pharm Sin B* 2023;13: 2403–24.
2. Aleksandrova K, Egea Rodrigues C, Floegel A, Ahrens W. Omics biomarkers in obesity: novel etiological insights and targets for precision prevention. *Curr Obes Rep* 2020;9:219–30.

3. Schwartz MW, Seeley RJ, Zeltser LM, Drewnowski A, Ravussin E, Redman LM, et al. Obesity pathogenesis: an endocrine society scientific statement. *Endocr Rev* 2017;**38**:267–96.
4. Gao L, Xu Z, Rao Y, Lu YT, Hu YT, Yu H, et al. Design, synthesis and biological evaluation of novel bouchardatine analogs as potential inhibitors of adipogenesis/lipogenesis in 3T3-L1 adipocytes. *Eur J Med Chem* 2018;**10**:90–101.
5. Tan TM. Co-agonist therapeutics come of age for obesity. *Nat Rev Endocrinol* 2023;**19**:66–7.
6. Newman DJ, Cragg GM. Natural products as sources of new drugs over the nearly four decades from 01/1981 to 09/2019. *J Nat Prod* 2020;**83**:770–803.
7. Pietiäinen M, Kontturi J, Paasela T, Deng XB, Ainasoja M, Nyberg P, et al. Two polyketide synthases are necessary for 4-hydroxy-5-methylcoumarin biosynthesis in *Gerbera hybrida*. *Plant J* 2016;**87**:548–58.
8. Catalán CAN, Borkosky SA, Joseph-Nathan P. The secondary metabolite chemistry of the subtribe gochnatiinae (tribe multiseieae, family Compositae). *Biochem Systemat Ecol* 1996;**24**:659–718.
9. Vestena AS, Meirelles GdC, Zuanazzi JA, Glv Poser. Taxonomic significance of coumarins in species from the subfamily Mutisioideae, Asteraceae. *Phytochem Rev* 2023;**22**:85–112.
10. Li T, Ma X, Fedotov D, Kjaerulff L, Frydenvang K, Coriani S, et al. Structure elucidation of prenyl- and geranyl-substituted coumarins in *Gerbera piloselloides* by NMR spectroscopy, electronic circular dichroism calculations, and single crystal X-ray crystallography. *Molecules* 2020;**25**:1706.
11. Wu ZL, Huang PL, Wang Q, Li JY, Sun ZS, Li HL, et al. Coumarin-monoterpenes from *Gerbera anandria* (Linn.) Sch.-Bip and their neuroprotective activity. *Bioorg Chem* 2022;**124**:105826.
12. Lei L, Xue YB, Liu Z, Peng SS, He Y, Zhang YY, et al. Coumarin derivatives from *Ainsliaea fragrans* and their anticoagulant activity. *Sci Rep* 2015;**5**:13544.
13. Flora of China Editorial Committee. *Flora reipublicae popularis sinicae*. Beijing: Science Press; 1996. p. 94.
14. Hong LY, Zhuo JX, Lei QY, Zhou JJ, Ahmed S, Wang CY, et al. Ethnobotany of wild plants used for starting fermented beverages in Shui communities of southwest China. *J Ethnobiol Ethnomed* 2015;**11**:42.
15. He F, Yang JF, Cheng XH, Wang R, Qu HC, Jiang HC, et al. 8-Methoxysmyrindiol from *Gerbera piloselloides* (L.) Cass. and its vasodilation effects on isolated rat mesenteric arteries. *Fitoterapia* 2019;**138**:104299.
16. Zhao CX, Gao H, Yu M, Zhao JP, He BX, Wu JP, et al. ¹H-NMR-guided isolation of enantiomeric coumarin-monoterpenes with anti-inflammatory activity from *Gerbera piloselloides*. *Phytochemistry* 2022;**203**:113346.
17. Shoyama Y, Takeuchi A, Taura F, Tamada T, Adachi M, Kuroki R, et al. Crystallization of Delta1-tetrahydrocannabinol acid (THCA) synthase from *Cannabis sativa*. *Acta Crystallogr, Sect F: Struct Biol Cryst Commun* 2005;**61**:799–801.
18. Zhao CX, Gao H, Li JR, Yu M, Wu JP, Zhang HX, et al. Bioactive constituents from *Gerbera piloselloides* with anti-inflammatory and antiproliferative activities. *Fitoterapia* 2022;**161**:105258.
19. Hubert C, Moreau J, Batany J, Duboc A, Hurvois JP, Renaud JL. Brønsted acid-catalyzed synthesis of pyrans via a formal [3+3] cycloaddition. *Adv Synth Catal* 2008;**350**:40–2.
20. Zhao CX, Gao H, Sun YJ, Huang YF, Zhang T, Zou ZM. Study on chemical constituents of *Gerbera piloselloides*. *Chin Tradit Pat Med* 2021;**43**:3061–7.
21. Zebisch K, Voigt V, Wabitsch M, Brandsch M. Protocol for effective differentiation of 3T3-L1 cells to adipocytes. *Anal Biochem* 2012;**425**:88–90.
22. Zhao X, Hu H, Wang C, Bai L, Wang Y, Wang W, et al. A comparison of methods for effective differentiation of the frozen-thawed 3T3-L1 cells. *Anal Biochem* 2019;**568**:57–64.
23. Lu T, Li Y, Lu W, Spitters T, Fang X, Wang J, et al. Discovery of a subtype-selective, covalent inhibitor against palmitoylation pocket of TEAD3. *Acta Pharm Sin B* 2021;**11**:3206–19.
24. Chen S, Li Z, Zhang S, Zhou Y, Xiao X, Cui P, et al. Emerging biotechnology applications in natural product and synthetic pharmaceutical analyses. *Acta Pharm Sin B* 2022;**11**:4075–97.
25. Gregoire FM, Smas CM, Sul HS. Understanding adipocyte differentiation. *Physiol Rev* 1998;**78**:783–809.
26. Luo H, Guo Y, Liu Y, Wang Y, Zheng R, Ban Y, et al. Growth differentiation factor 11 inhibits adipogenic differentiation by activating TGF-beta/Smad signaling pathway. *Cell Prolif* 2019;**52**:e12631.
27. Nishino N, Tamori Y, Tateya S, Kawaguchi T, Shibakusa T, Mizunoya W, et al. FSP27 contributes to efficient energy storage in murine white adipocytes by promoting the formation of unilocular lipid droplets. *J Clin Invest* 2008;**118**:2808–21.
28. Brasaemle DL. Thematic review series: adipocyte biology. The perilipin family of structural lipid droplet proteins: stabilization of lipid droplets and control of lipolysis. *J Lipid Res* 2007;**48**:2547–59.
29. Gesta S, Tseng YH, Kahn CR. Developmental origin of fat: tracking obesity to its source. *Cell* 2007;**131**:242–56.
30. Rosen ED, Hsu CH, Wang X, Sakai S, Freeman MW, Gonzalez FJ, et al. C/EBPα induces adipogenesis through PPARγ: a unified pathway. *Genes Dev* 2002;**16**:22–6.
31. Kersten S. Mechanisms of nutritional and hormonal regulation of lipogenesis. *EMBO Rep* 2001;**2**:282–6.
32. Anthonen MW, Rönstrand L, Wernstedt C, Degerman E, Holm C. Identification of novel phosphorylation sites in hormone-sensitive lipase that are phosphorylated in response to isoproterenol and govern activation properties *in vitro*. *J Biol Chem* 1998;**273**:215–21.
33. Lass A, Zimmermann R, Oberer M, Zechner R. Lipolysis—a highly regulated multi-enzyme complex mediates the catabolism of cellular fat stores. *Prog Lipid Res* 2011;**50**:14–27.